

Cite this: *Digital Discovery*, 2026, 5,
1351

MSIGN: A deep learning framework based on multi-scale interaction graph neural networks for predicting binding of synthetic cannabinoids to receptors

Zhenyong Cheng,^{†a} Dinghao Liu,^{†a} Yuanpeng Fu,^{†a} Kewei Sheng,^a Yan Xing,^a
Yanling Qiao,^{bcd} Shangxuan Cai,^{ef} Jubo Wang,^d Peng Xu,^{bcd} Bin Di,^{cd}
and Jun Liao^{id *acg}

Deep learning-based models have been extensively applied to the task of protein–ligand binding affinity (PLA) prediction. Current 3D ligand-complex-based GNNs, though advanced, still struggle with accuracy and generalization due to their overreliance on atomic-level physical features and their neglect of chemical space dynamics, leading to data memorization rather than robust learning. To address these issues, we propose a deep learning model based on a Multi-Scale Interaction Graph Neural Network (MSIGN). By constructing ligand functional group graphs and protein amino acid graphs, we introduce chemical information features into the model, which are combined with physical features to enhance binding affinity prediction. Especially, we innovatively adopt a pre-training and fine-tuning training approach in the PLA domain to improve the model's generalization capability on downstream tasks (this study focuses on the binding affinity prediction of synthetic cannabinoids), and we validated the MSIGN model predictions with wet experiments such as SPR on three novel synthetic cannabinoids. Furthermore, we analyze the impact of different fine-tuning strategies on the model's generalization ability. Multiple results collectively demonstrate the superiority of our MSIGN model design, providing a novel approach for future PLA prediction.

Received 18th July 2025
Accepted 15th February 2026

DOI: 10.1039/d5dd00317b

rsc.li/digitaldiscovery

1. Introduction

Driven by the exponential growth of structural and binding data, AI-based protein–ligand affinity prediction has advanced rapidly.^{1–5} Current representation methods are categorized into 3D-independent and 3D-dependent approaches. 3D-independent methods include 1D sequence-based models, such as DeepGLSTM,^{2,6,12} which capture residue-level context, and 2D graph-based representations.^{7–11} Among them, SIGN¹³ utilizes the Graph Attention Mechanism (GAT) to model atomic

interactions between protein residues and ligand atoms. To better reflect binding dynamics, models like EGNA,¹⁴ further integrate spatial distances into dynamic interaction graphs, bridging the gap between topological information and 3D spatial relationships.

Despite their utility, 1D and 2D representations often neglect critical 3D spatial interactions.¹⁵ To address this, 3D-dependent methods like voxel-based approaches^{16–20} extract features from atomic coordinates; however, they often fail to capture explicit interatomic bonding or align with real-world physical principles.²¹ Consequently, 3D graph structures, which enrich 2D topologies with spatial distance and angle information, have emerged as the mainstream approach for more precise feature representation.

Recent studies reveal that models trained on atomic features often capture dataset biases rather than fundamental physical principles,¹⁵ frequently over-relying on ligand structures while neglecting protein–ligand interactions. To enhance generalizability and interpretability, Moon *et al.*²¹ integrated physical priors by decomposing binding affinity into specific pairwise interactions (*e.g.*, van der Waals forces and hydrogen bonds). Building on this, Yang *et al.*²² introduced a learnable bias correction term to further mitigate hidden systematic biases in the data.

^aSchool of Science, China Pharmaceutical University, Nanjing 211198, China. E-mail: liaojun@cpu.edu.cn; Tel: +086-86185160^bKey Laboratory of Drug Monitoring and Control, Drug Intelligence and Forensic Center, Ministry of Public Security, Beijing 100193, China^cOffice of China National Narcotics Control Commission, China Pharmaceutical University Joint Laboratory on Key Technologies of Narcotics Control, Beijing 100193, China^dSchool of Pharmacy, China Pharmaceutical University, Nanjing 211198, China^eState Key Laboratory of Membrane Biology, Peking University School of Life Sciences, Beijing 100871, China^fPKU-IDG/McGovern Institute for Brain Research, Beijing 100871, China^gZhejiang Lab, Hangzhou 311500, China[†]Zhenyong Cheng and Dinghao Liu are co-first authors.

While atom-centric methods provide fundamental structural insights,²³ they struggle to capture higher-level functional similarities or the distribution of complexes in chemical space. To address these limitations, we propose a multi-scale model integrating physical and chemical priors. By incorporating molecular functional groups^{24,25} and amino acid residues,²⁶ our model moves beyond individual atoms to capture essential chemical properties—such as reactivity, polarity, and hydrophobicity—that fundamentally govern protein–ligand interaction patterns.

Despite the success of deep learning in virtual screening, data dependency remains a significant bottleneck for targets with limited experimental data, such as G protein-coupled receptors (GPCRs).²⁷ Cannabinoid receptor 1 (CB1R), a classical GPCR predominantly expressed in the brain, mediates critical central nervous system effects. Synthetic cannabinoids (SCs) act as potent full agonists of CB1R, exhibiting stronger psychoactive and addictive properties than their natural counterparts. Given that SC-CB1R affinity directly correlates with addictive potential, its accurate prediction is essential for pharmacological risk assessment.

To overcome the generalization limits of small-sample datasets,²⁸ we propose a transfer learning strategy based on a pre-training and fine-tuning paradigm. A generalized MSIGN model is first pre-trained on the PDBbind dataset to capture fundamental laws of protein–ligand interactions. Subsequently, the model is fine-tuned on a specialized CB1R-SC dataset curated from BindingDB to acquire domain-specific knowledge. Wet-lab experiments, including SPR and fluorescence assays on three novel SCs, further validate that this multi-scale approach effectively bridges the gap between general physical rules and specific biological activity. In summary, the main contributions of this work are as follows:

(i) Multi-scale graph design: we propose MSIGN, a multi-scale framework that integrates atomic interaction graphs with ligand functional group and protein residue graphs. This design effectively fuses physical interaction features with chemical priors, enhancing both model accuracy and interpretability.

(ii) Systematic fine-tuning strategy: we conducted a comprehensive evaluation of transfer learning paradigms (General, No-pretraining, Frozen, and Full Fine-tuning). We demonstrate that the “pre-training + full fine-tuning” strategy is critical for overcoming domain shifts and achieving generalization in data-scarce GPCR tasks.

(iii) Experimental validation and benchmarking: we validated the model’s practical utility through the wet-lab synthesis and biological assay of three novel synthetic cannabinoids. Cross-method benchmarking confirms that MSIGN achieves superior consistency with experimental results compared to physics-based docking and other state-of-the-art deep learning models.

2. Experimental

The methodological framework of our MSIGN is systematically illustrated in Fig. 1. We provide a comprehensive description of

the pipeline, spanning dataset construction, feature engineering, and model architecture, with particular emphasis on the methodologically rigorous integration of physical-chemical priors and multi-scale representations.

2.1 Dataset

This study utilized two public datasets, PDBbind v2020 (ref. 29) and BindingDB,³⁰ to acquire general protein–small molecule ligand binding affinity data and CB1 receptor ligand binding affinity data, respectively. The distribution of labels for these two datasets is shown in Fig. 2A and B.

2.1.1 General protein–ligand binding dataset. For the binding affinity prediction task, we train and validate the proposed MSIGN model on the general set of PDBbind v2020, in line with other benchmark models. We collate a total of 14 127 complexes with experimentally determined binding affinities from the PDBbind website, wherein the binding affinities are represented as $-\log K_d$, $-\log K_i$, or $-\log IC_{50}$ (with larger values indicating stronger binding). Complexes were removed by matching PDB IDs against the CASF-2013, CASF-2016, and CASF-2019 core lists prior to dataset splitting to ensure absolutely no data leakage. We then exclude samples that cannot be parsed by RDKit and randomly partition the remaining samples into training ($N = 11\,904$) and validation ($N = 1000$) sets. To test MSIGN’s generalization capability, we leverage three independent external test sets: the CASF-2013 benchmark, the CASF-2016 benchmark, and the 2019 core set. It should be noted that there is no overlap among training, validation, and testing sets.

2.1.2 CB1R-ligand binding dataset. CB1R-specific binding affinity data (K_d , K_i , and IC_{50}) were retrieved from BindingDB, targeting *CNR1_HUMAN* based on PDB templates 5TGZ, 5XR8, 5XRA, and 7WV9.^{31–33} Starting from 5541 raw entries, we performed rigorous curation: removing exact duplicates, averaging affinities for identical SMILES (848 cases), and excluding 27 problematic docking data points. The final dataset, SCsDB, comprises 4166 unique ligand–affinity pairs (Fig. S1). For model fine-tuning, the data were split into training and validation sets at an 8 : 2 ratio.

2.2 Feature representation

This study employs three distinct types of graph structures: the complex atomic interaction graph, the SC functional group graph, and the CB1R ligand amino acid residue graph. These graphs are designed to explore the feature space of SC-CB1R binding interactions from three perspectives: 3D structural information, physical principles, and chemical properties; all feature dimensions are shown in Tables S1–S3. The following sections provide detailed descriptions of these graph structures.

2.2.1 Protein–ligand complex atomic interaction graph. In this study, the SC-CB1R complex is represented as a 3D graph structure. The atoms constituting both SCs and CB1R serve as two types of node features in the graph. The edges of the graph are composed of covalent interactions between SC atoms, covalent interactions between CB1R atoms, and non-covalent interactions between SC and CB1R atoms. Formally, the 3D graph is defined as $G=(V, E)$, where



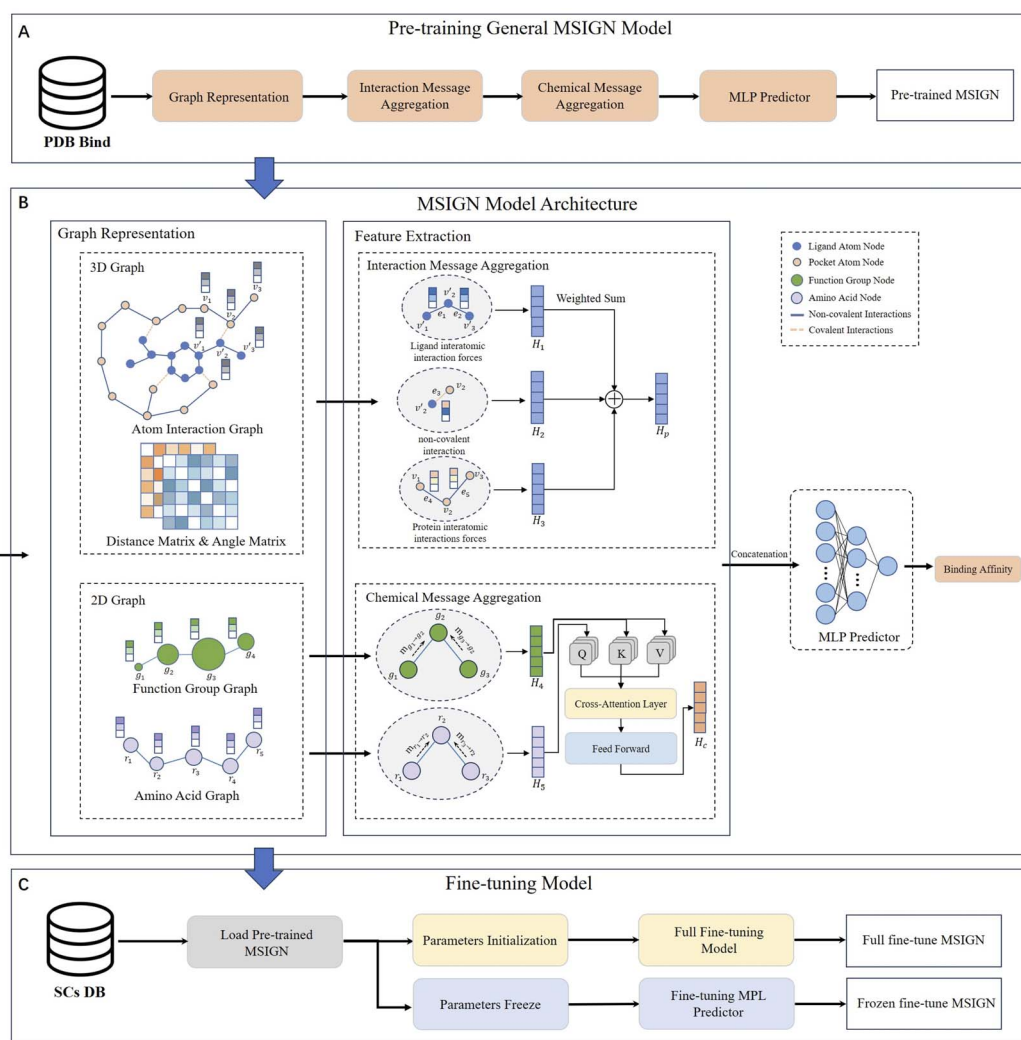


Fig. 1 Illustration of the basic framework of the MSIGN model. (A) Pre-training process of MSIGN on the general dataset PDBbind. (B) Overall architecture of the MSIGN model, comprising a graph representation module, a Feature Extraction module, and an MLP Predictor module. (C) Application of two fine-tuning strategies—full fine-tuning and frozen fine-tuning—to adapt the pre-trained MSIGN model for transfer learning on the SCsDB dataset, leveraging knowledge from general binding affinity prediction.

$V = \{v_n, v'_m | n, m \in [1, 2, \dots, N]\}$ and $E = \{e_i, e_j | i, j \in [1, 2, \dots, M]\}$. Here, V represents the set of atoms, including SC atoms v_n and CB1R atoms v'_m , with N being the total number of atoms in the complex. EE denotes the set of edges, comprising two types of interactions: covalent bonds e_i and non-covalent bonds e_j .

2.2.2 Functional group graph and amino acid residue graph. Inspired by Shen Han *et al.*,²⁵ a 2D functional group graph was constructed for SCs where nodes represent distinct functional groups and edges denote their chemical connectivity. For CB1R, an amino acid residue graph was built with nodes representing the 20 residue types. Residue–residue interactions are defined by a 5 Å distance threshold between $C\alpha$ atoms in 3D space, resulting in an $n \times n$ adjacency matrix based on spatial contact.^{34,35}

2.3 Model architecture

2.3.1 Multi-scale interaction graph neural network (MSIGN). Our proposed MSIGN integrates physical and

chemical prior knowledge to perform feature interaction and fusion across multiple scales:

(1) Atomic-Level 3D interaction features: MSIGN constructs an atomic-level graph representation of the 3D complex formed by the ligand and the target protein's binding pocket. Through a message-passing network, it iteratively updates edge features by aggregating node embeddings from neighboring atoms. This process ultimately quantifies both covalent and non-covalent interactions between atoms.

(2) Functional group and amino acid-level 2D property features: in contrast to the atomic-level graph structure, proteins and ligands are modeled as 2D functional group graphs and amino acid residue graphs, respectively. By incorporating these multi-scale features, MSIGN captures both fine-grained atomic interactions and higher-level chemical characteristics, enhancing its ability to predict binding affinities accurately.

2.3.2 Message passing neural networks on graphs. Since Gilmer *et al.*³⁶ summarized the Message Passing Neural



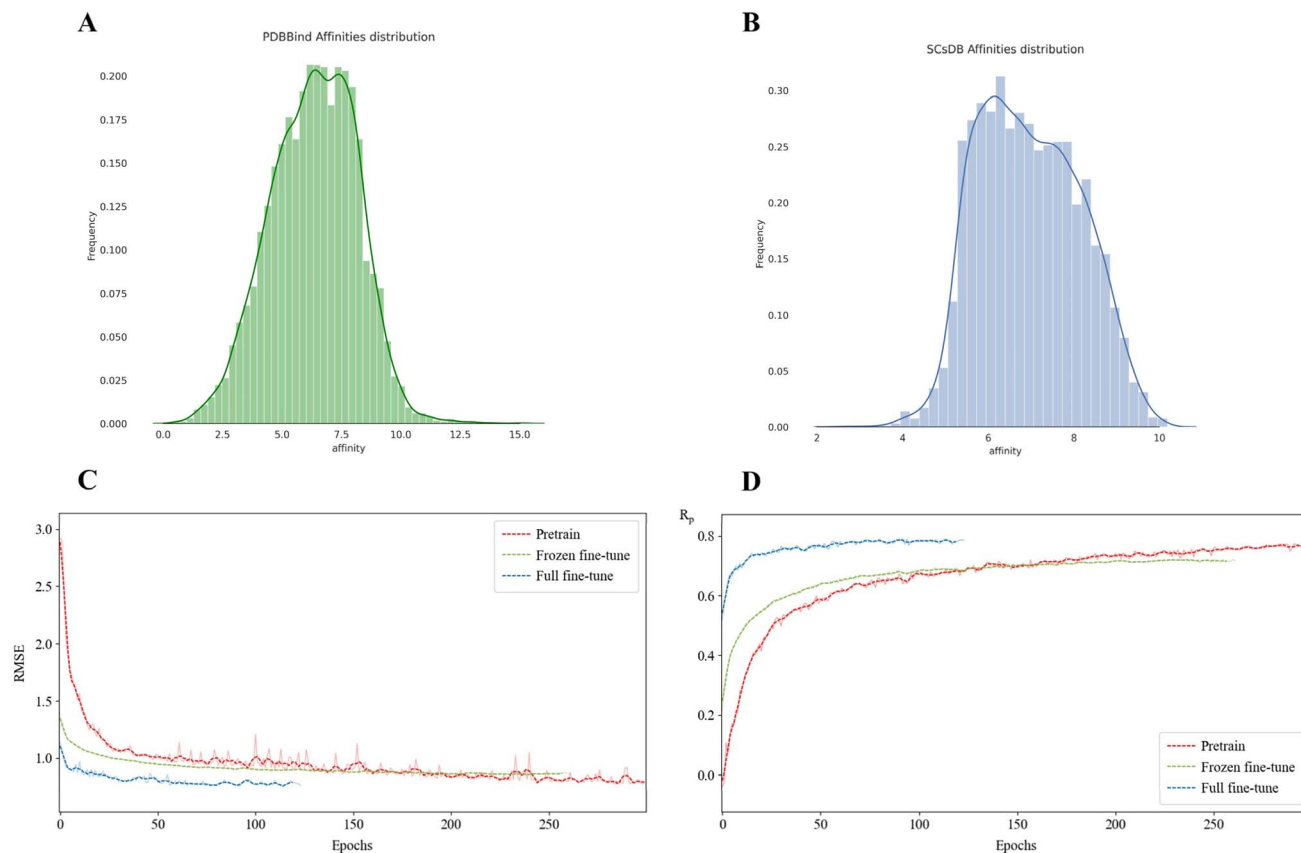


Fig. 2 Transfer learning dataset and training process. (A) Distribution of protein–ligand binding affinity labels on the general dataset PDBbind. (B) Distribution of labels on the constructed CB1R-SCs binding affinity dataset. (C) Validation set RMSE. (D) Validation set R_p .

Network (MPNN), a supervised learning framework designed for graph-structured data, it is gradually becoming the most dominant approach for a variety of molecular related tasks, such as molecular representation^{37,38} and molecular property prediction.^{39,40} The feature extraction method of our MSIGN model is constructed precisely on the basis of the MPNN framework. It consists of two key forward propagation phases: the message-passing phase and the readout phase. The primary objective of the message-passing phase is to generate messages based on node features (Node Feature) and propagate these messages according to the graph's topological structure. For a node v in graph G , its vector representation h_v is updated iteratively as follows:

$$m_v^{t+1} = \sum_{u \in N(v)} M_t(h_v^t, h_u^t, e_{uv}^t) \quad (1)$$

$$h_v^{t+1} = U_t(h_v^t, m_v^{t+1}) \quad (2)$$

Here, $M_t()$ denotes the message function, which generates messages based on node features (h_v^t , h_u^t), edge features (e_{uv}^t), and the adjacency relationships of the graph. $u \in N(v)$ represents the set of neighboring nodes u adjacent to node v . $U_t()$ is the aggregation function, which updates the node's feature representation by combining its current state h_v^t with the aggregated message m_v^{t+1} .

The readout phase aims to map the entire graph's features into a global feature vector that captures the graph's holistic properties. This is achieved using a readout function:

$$\hat{y} = R(\{h_v^T | v \in G\}) \quad (3)$$

Here, $R()$ denotes the permutation-invariant readout function, which operates on all node states h_v^T (final layer representations) to generate a graph-level feature vector.

2.3.3 Feature extraction module based on atomic interactions. As mentioned earlier, inspired by the work of Seokhyun Moon *et al.*,²¹ this study decomposes the interactions between SCs and the CB1R into the sum of covalent and non-covalent interactions between their constituent atoms. As shown in Fig. 1B, we designed an atomic interaction-based feature extraction module to separately extract covalent interactions among SC atoms, covalent interactions among CB1R atoms, and non-covalent interactions between SCs and CB1R atoms.

Specifically, to calculate the strength of covalent interactions among CB1R binding pocket atoms, we take atom v_i as an example: first, we query the adjacency matrix of the graph to identify all neighboring atoms v_j of v_i . The feature matrices of these neighboring nodes and the edge features are processed through a message function to generate a message m_{v_j} , which is then propagated to node v_j . An aggregation function combines



the previous layer's h_{v_i} with the message m_{v_i} to obtain the feature H_1 . The mathematical representation is as follows:

$$h_v^{t+1} = g \left(h_v^t, \sum_{v_j \in N(v_i)} f_{\theta} \left(h_{v_i}^t, h_{v_j}^t, e_{v_i v_j}^t \right) \right) \quad (4)$$

$$H_1 = \sigma \left(\sum_{i=1}^N W_{\alpha} h_v^t \right), W_{\alpha} \in R^{n \times n} \quad (5)$$

Here, v_i and v_j represent SC atom nodes, with v_j being a neighbor of v_i . $e_{v_i v_j}^t$ denotes the edge feature connecting v_i and v_j at layer t , while $h_{v_i}^t$ and $h_{v_j}^t$ are the feature tensors of atoms v_i and v_j at layer t , respectively. $f_{\theta}()$ is a message function with learnable parameters θ , and $g()$ is the aggregation function, which we choose to be the sum function. W_{α} is a learnable weight matrix.

The covalent interactions among SC atoms are computed similarly, with the atom node set replaced by SC atoms. The equations are as follows:

$$h_v^{t+1} = g \left(h_v^t, \sum_{v_k \in N(v_i)} f_{\theta} \left(h_{v_i}^t, h_{v_k}^t, e_{v_i v_k}^t \right) \right) \quad (6)$$

$$H_2 = \sigma \left(\sum_{i=1}^N W_{\alpha} h_v^t \right), W_{\alpha} \in R^{n \times n} \quad (7)$$

Due to the significantly larger number of non-covalent interactions compared to covalent interactions, we employ mean aggregation for non-covalent interaction calculations. The equations are as follows:

$$h_{w'}^{t+1} = g \left(h_{w'}^t, \sum_{v' \in N(v)} f_{\theta} \left(h_v^t, h_{v'}^t, e_{v v'}^t \right) \right) \quad (8)$$

$$H_3 = \sigma \left(\frac{1}{N} \sum_{i=1}^N W_{\alpha} h_{w'}^t \right), W_{\alpha} \in R^{n \times n} \quad (9)$$

2.3.4 Feature extraction module based on functional groups and amino acid residues. While atomic-level classification provides a fundamental understanding of molecular structures, it is insufficient for analyzing large or complex molecules, as it fails to directly reflect chemical functionality and reactivity, potentially leading the model astray. To address this, we introduce functional group-level features to complement atomic features. Incorporating functional group features helps the model learn molecular chemical functions and potential bioactivity, thereby enhancing the interpretability of binding affinity prediction tasks.

Similarly, to comprehensively analyze the chemical properties of the CB1R protein, we construct and incorporate an amino acid residue graph. Amino acid residues in proteins exhibit diverse chemical properties, such as polarity, hydrophobicity, and charge, which determine protein–ligand interaction patterns.

For the constructed CB1R amino acid residue graph and ligand functional group graph, we perform one iteration of message passing to aggregate features from neighboring nodes and generate messages, ultimately obtaining tensor representations of the entire protein and molecule. These features are then fed into a cross-attention layer to learn potential global correspondences. The cross-attention computation is as follows:

$$Q = M_f W^Q, K = M_a W^K, V = M_a W^V \quad (10)$$

$$H_c = \text{Cross attention}(Q, K, V) = \text{softmax} \left(\frac{QK^T}{\sqrt{d_K}} \right) V \quad (11)$$

Here, M_f and M_a represent the functional group feature tensor and amino acid residue feature tensor obtained from the message-passing layer, respectively. W^Q , W^K , and $W^V \in R^{d \times d_K}$ are projection matrices, and $\text{softmax}()$ is the function used to compute attention scores.

2.3.5 Loss function construction and final prediction. The predicted value of MSIGN is composed of two parts: the physical prior knowledge and chemical prior knowledge extracted from the feature extraction modules:

$$\hat{y}_{\text{pred}} = \text{MLP}(\text{concat}(H_p, H_c)) \quad (12)$$

$$L_{\text{mse}} = \frac{1}{N} \sum_{n=1}^N |y_n - \hat{y}_n|^2 \quad (13)$$

Here, $H_p \in R^m$ represents the abstracted physical rules learned by the model, and $H_c \in R^n$ represents the abstracted chemical rules. These are concatenated and fed into a multilayer perceptron (MLP), after which the loss function L_{mse} is computed against the true labels and used for backpropagation.

2.4 Implementation details

The MSIGN framework was implemented using PyTorch and PyTorch Geometric. All experiments were performed on a workstation equipped with a single NVIDIA GeForce RTX 4090 GPU. The model utilizes an Adam optimizer with a learning rate of 1×10^{-4} and a weight decay of 1×10^{-6} . The batch size was set to 128, and the training was conducted for a maximum of 300 epochs with an early stopping strategy (patience set to 30 epochs) to prevent overfitting. The model architecture consists of 3 message-passing layers with a hidden feature size of 256. The pre-training process is computationally efficient, requiring approximately 5 GB of GPU memory and completing in about 3.5 hours.

3. Results and discussion

3.1 Comparison of general MSIGN with baseline models

The MSIGN model architecture (as shown in Fig. 1) has demonstrated excellent performance in both the general model trained on the PDBbind dataset and the transfer learning model trained on the SC dataset. To rigorously evaluate the superiority of the general MSIGN model, we selected representative baseline models for comparison, including DeepDTA,⁶



MGraphDTA,⁴¹ Pafnucy,¹⁷ GIGN,³ SS-GNN,⁴² and EHIGN.²² Additionally, to provide a broader context, we implemented classical machine learning models, Random Forest (RF) and XGBoost, as baselines.

Table 1 and Table S4 below summarizes the performance comparison between MSIGN and other baseline models on the CASF-2013,⁴³ CASF-2016,⁴⁴ and 2019 core set benchmark test sets. The evaluation metrics used are Root Mean Square Error (RMSE) and Pearson correlation coefficient (R_p). To better quantify the model advancement and assess statistical significance, we calculated 95% confidence intervals (CI) for MSIGN and the machine learning baselines. These intervals were derived using a non-parametric bootstrap resampling procedure, as recommended for rigorous model validation.⁴⁵ Specifically, prediction–target pairs were resampled with replacement 10 000 times, and the 2.5th and 97.5th percentiles of the resulting metric distributions were taken as the confidence bounds. The results indicate that MSIGN achieved the best performance across all metrics on all test sets. This superior performance underscores the effectiveness of MSIGN in capturing both atomic-level interactions and higher-level chemical features, demonstrating its robustness and generalizability in binding affinity prediction tasks.

3.2 Ablation study and permutation analysis

To systematically evaluate the contributions of each feature component and verify whether MSIGN truly learns physical interactions rather than exploiting dataset biases, we conducted both feature ablation studies and permutation-based control tests.

Feature ablation analysis: we designed four MSIGN variants by selectively removing the Atomic Interaction Graph (IG), Ligand Functional Group Graph (FG), or Amino Acid Residue Graph (AARG). As summarized in Table 2, the full MSIGN model consistently outperforms all variants. The model relying solely on IG (MSIGN_IG) shows suboptimal performance, while removing IG entirely (MSIGN_FG + AARG) leads to the worst results, confirming that atomic interactions form the physical

foundation of binding. The integration of chemical priors (FG and AARG) significantly boosts performance, with the full model achieving the lowest validation RMSE and highest correlation. These results demonstrate the synergistic effect of fusing multi-scale physical and chemical features.

Permutation-based control tests: to verify that MSIGN captures genuine 3D interactions rather than dataset biases,^{46,47} we conducted permutation tests (Table 3). Shuffling ligand labels (ligand permutation) caused a complete performance collapse, confirming the model's sensitivity to ligand identity. In the protein permutation setting, although the model retained moderate correlation due to intrinsic ligand potency, its performance degraded significantly, dropping even below that of the ligand-only ML baselines. This observation is critical: it rules out the possibility that MSIGN acts merely as a ligand-based predictor, which would otherwise maintain baseline-level accuracy despite protein shuffling. Instead, MSIGN achieves state-of-the-art performance only when genuine protein–ligand pairs are preserved. This substantial performance gap between the permuted and original settings validates the atomic interaction graph module, confirming that the model's predictive power stems from learning specific 3D spatial complementarity rather than exploiting ligand or protein priors.

3.3 Performance of general MSIGN models on GPCR families

We first compiled 1417 GPCR entries with PDB identifiers by combining datasets from InterPro⁴⁸ and GPCRdb.⁴⁹ Subsequent

Table 2 Comparison of different MSIGN model variants in terms of metrics

Model variant/setting	IG	FG	AARG	RMSE	R_p
MSIGN_IG	✓	✗	✗	1.353	0.701
MSIGN_FG + AARG	✗	✓	✓	1.401	0.654
MSIGN_IG + FG	✓	✓	✗	1.263	0.719
MSIGN_IG + AARG	✓	✗	✓	1.268	0.723
MSIGN	✓	✓	✓	1.219	0.747

Table 1 Comparison of performance metrics between MSIGN and all baseline models on three test sets

Model	CASF-2013		CASF-2016		2019 core set	
	RMSE	R_p	RMSE	R_p	RMSE	R_p
DeepDTA ^a	1.651	0.713	1.363	0.781	1.503	0.589
MGraphDTA ^a	1.737	0.682	1.454	0.742	1.533	0.529
Pafnucy ^a	1.523	0.779	1.438	0.771	1.441	0.617
GIGN ^a	1.384	0.819	1.188	0.843	1.399	0.637
SS-GNN ^a	1.327	0.826	1.172	0.848	1.452	0.629
EHIGN ^a	1.308	0.841	1.156	0.853	1.363	0.664
Random forest ^b	1.775 [1.538, 2.009]	0.661 [0.533, 0.766]	1.622 [1.478, 1.768]	0.651 [0.571, 0.722]	1.499 [1.467, 1.531]	0.544 [0.521, 0.566]
XGBoost ^b	1.588 [1.382, 1.786]	0.749 [0.648, 0.828]	1.448 [1.318, 1.575]	0.742 [0.678, 0.796]	1.466 [1.434, 1.498]	0.580 [0.559, 0.601]
MSIGN ^b	1.256 [1.114, 1.419]	0.848 [0.808, 0.899]	1.130 [1.042, 1.214]	0.857 [0.834, 0.891]	1.327 [1.301, 1.344]	0.673 [0.647, 0.684]

^a Results for DeepDTA, MGraphDTA, Pafnucy, GIGN, SS-GNN, and EHIGN were retrieved directly from the literature [ref], where confidence intervals were not reported. ^b For Random Forest, XGBoost, and MSIGN, values represent the observed metric followed by the [95% Confidence Interval] in brackets. The intervals were calculated using bootstrap resampling with 10 000 iterations, based on the 2.5th and 97.5th percentiles of the distribution.



Table 3 Performance comparison under permutation-based control settings to assess the model's reliance on genuine protein–ligand interactions

Experimental setting	CASf-2013		CASf-2016		2019 core set	
	RMSE	R_p	RMSE	R_p	RMSE	R_p
Ligand permutation	3.097	0.0478	2.717	0.177	2.640	0.096
Protein permutation	2.126	0.599	2.040	0.542	2.278	0.388
Joint permutation	3.508	−0.168	2.941	−0.025	2.834	0.019
Original (baseline)	1.256	0.848	1.130	0.857	1.327	0.673

intersection with PDBbind entries yielded 48 GPCR protein–ligand complexes, which were isolated as an external test set. The remaining data (excluding these 48 GPCR entries) was partitioned into training and validation sets at an 8:2 ratio. Using identical hyperparameters to previous configurations, we trained a new MSIGN model by minimizing the RMSE on the validation set and then evaluated its performance on the GPCR test set. The first 15 results (sorted in ascending order according to affinity label size) are shown in Table 4, with the bold part indicating that the absolute value of the difference is greater than 0.5.

Experimental results revealed an RMSE of 1.5626 and a correlation coefficient of 0.2705 between predicted and actual values. This demonstrates that limited training data severely impede the model's ability to capture interaction patterns between ligands and mechanistically complex protein families like GPCRs, with most predictions deviating substantially from experimental observations. To address this challenge for accurate prediction of CB1R-SC interactions, we propose implementing a pre-training and transfer learning framework for deeper investigation.

3.4 Transfer learning with MSIGN

The scarcity and specialization of synthetic cannabinoid (SC) data present a significant challenge for model generalization. To overcome this, we implemented a transfer learning

Table 4 Comparison of the predicted and true values of GPCR–ligand complexes

	PDB ID	Label	Predicted value	Difference
1	5k5s	2.69	4.94	2.25
2	3c14	3.52	4.65	1.13
3	5vex	4.63	6.59	1.96
4	5vew	5.15	6.98	1.83
5	3eht	5.17	5.64	0.47
6	4mk0	5.20	7.75	2.55
7	1y3a	5.41	7.04	1.63
8	6d1u	5.44	6.44	1.00
9	1cs4	5.57	4.53	−1.04
10	2g83	5.92	7.37	1.45
11	5ukl	6.20	7.64	1.44
12	5ukk	6.21	7.93	1.72
13	3rbq	6.27	6.36	0.09
14	4wnk	6.42	8.85	2.43
15	3 d7m	6.44	6.32	−0.12

paradigm (Fig. 2A and B) to bridge the gap between general physicochemical laws and domain-specific binding modes. This strategy addresses two critical bottlenecks: (i) the chemical space bias inherent in generalized models when applied directly to SCs–CB1R interactions and (ii) the high risk of overfitting when training on a limited dataset of only a few thousand entries. By first capturing fundamental interactions (*e.g.*, hydrogen bonding and hydrophobic complementarity) from the PDBbind dataset, the model subsequently learned to adapt to unique SC–CB1R features, such as the preference of indolyl ring orientation and residue polarity distribution.

Comparative analysis of different fine-tuning strategies (Fig. 2C and D and S2) highlights the necessity of this approach. Training MSIGN directly on the SCsDB without pre-training resulted in the longest training duration, significant RMSE fluctuations, and poor stability, indicating a failure to converge effectively. In contrast, while the “frozen” strategy reduced training time, the full fine-tuning strategy demonstrated superior performance. It achieved the lowest validation RMSE and reached convergence in only 124 epochs (Fig. S3 and S4). These results underscore that the “pre-training + full fine-tuning” framework not only optimizes computational efficiency but also significantly enhances the model's ability to generalize across the novel chemical spaces of synthetic cannabinoids.

3.5 Experimental verification of the reliability of model predictions

In affinity prediction, mixing K_i , K_d , and IC_{50} labels (converted to pK) is a common but debated practice due to potential systematic errors arising from different experimental conditions. To evaluate this effect, we compared our hybrid model (MSIGN_Mix) against sub-models trained on the K_i subset ($N = 2916$) and the IC_{50} subset ($N = 1215$) (Fig. S5; K_d was excluded due to $N = 35$). As shown in Table S5, MSIGN_Mix demonstrated the best performance, achieving the lowest RMSE and the highest correlation R_p (0.790).

This suggests that label hybridization enhances performance by expanding the training data and neutralizing metric-specific noise. Interestingly, MSIGN_ IC_{50} outperformed MSIGN_ K_i in R_p , likely because IC_{50} experiments often use more standardized conditions (*e.g.*, fixed enzyme/substrate concentrations), whereas K_i values may exhibit higher heterogeneity due to variable competitive inhibition assay setups. Despite these intrinsic differences, the superior accuracy of MSIGN_Mix indicates that the model effectively captures universal protein–ligand binding mechanisms that transcend specific experimental metrics.

3.6 Experimental verification of model predictions

To assess the practical reliability of the fine-tuned MSIGN model, we performed functional validation on three novel synthetic cannabinoids (SCs) through fluorescence-based sensing and SPR assays.

3.6.1 Biological evaluation via the GRABeCB2.5 sensor. To evaluate the physiological activation of CB1R by these novel SCs, we employed a stable HEK293T cell line expressing the



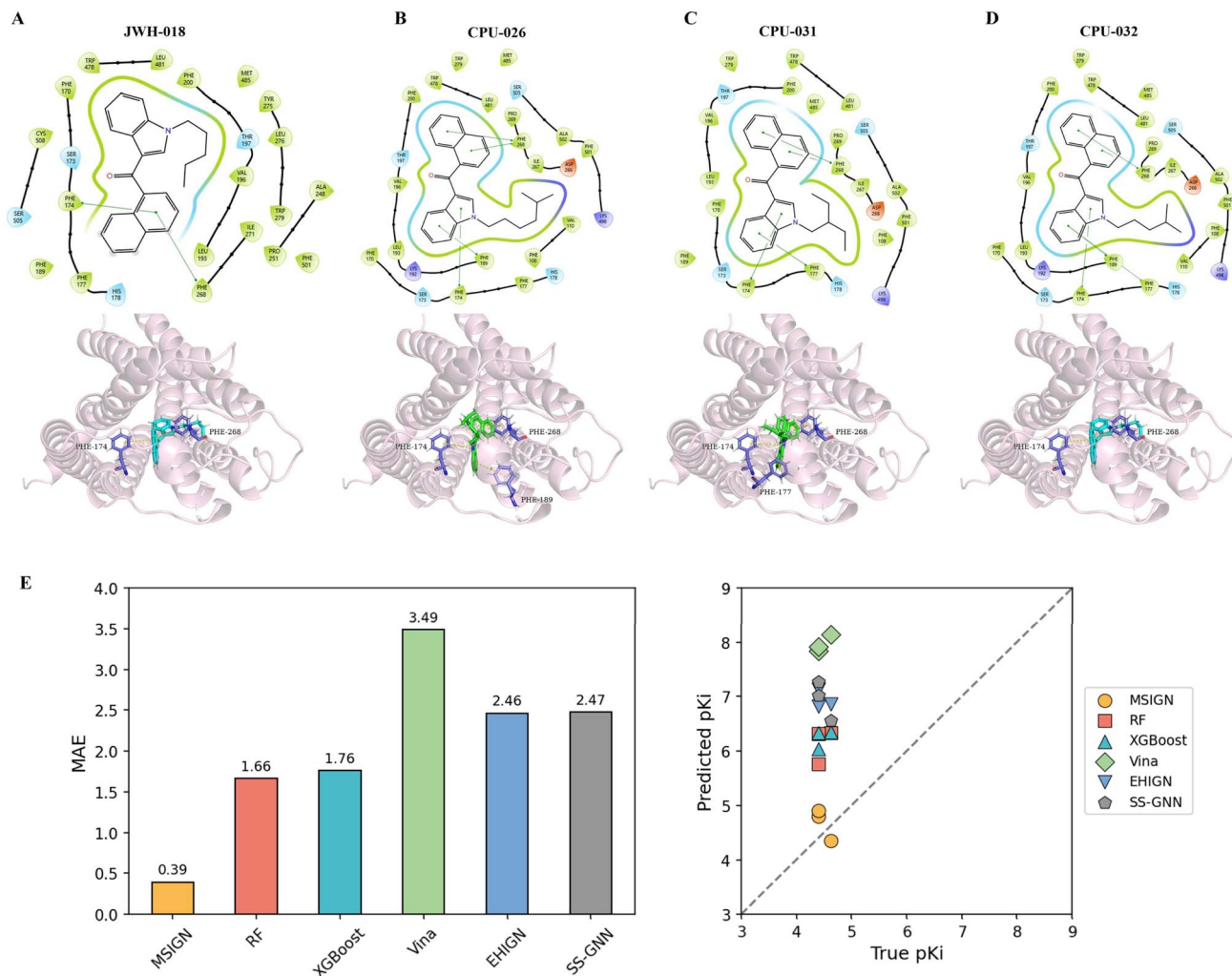


Fig. 3 Structural binding modes and predictive accuracy validation of novel synthetic cannabinoids (SCs). (A–D) 2D interaction diagrams and 3D binding poses of the reference JWH-018 and three novel SCs (CPU-026, CPU-031, and CPU-032) within the CB1R binding pocket. (E) Benchmarking of the predictive performance of MSIGN against baseline models on the three novel compounds.

endocannabinoid sensor GRABeCB2.5. This GPCR-based sensor converts the conformational change of CB1R upon ligand binding into a measurable green fluorescence signal, providing a real-time readout of receptor activation. The sensor-expressing stable cell line was generated using a hyperactive piggyBac transposase system to ensure robust and consistent expression.^{50,51}

3.6.2 Fluorescence imaging and efficacy assessment. The cells were imaged using a high-content screening system (Operetta CLS), and the physiological responses were quantified using the change in fluorescence intensity ($\Delta F/F_0$). Upon administration of the predicted SCs *via* bath application, we observed significant fluorescence responses, indicating that the novel compounds effectively triggered CB1R activation.

As shown in Fig. S6 and S7, the dose–response curves obtained from these fluorescence assays serve as critical physiological “ground truth.” These results, along with the K_d values measured by SPR, were used to externally validate the predictive accuracy of our MSIGN model. The high consistency between the

AI-predicted affinities and these biological responses (discussed in Section 3.7) demonstrates that MSIGN successfully captured the structural nuances required for CB1R–ligand interaction.

3.7 Full finetuning of the MSIGN model achieves optimal predictions

To evaluate the practical predictive power of MSIGN, we conducted a validation using three novel synthetic cannabinoids (SCs) confirmed by wet-lab experiments. We first compared four internal training paradigms (Fig. S8 and Tables S6 and S7). The General model showed a pronounced systematic overestimation, failing to capture the specific CB1R pocket interaction due to “domain shift.” Conversely, the no-pretraining model exhibited an underestimation trend, suggesting that small-domain datasets alone are insufficient to learn fundamental physical laws, leading to underfitting. While frozen fine-tuning partially reduced these errors, it remained constrained by parameter fixation. Ultimately, the full fine-tuning strategy achieved the highest consistency with experimental measurements,



demonstrating that full-parameter updates are essential for capturing target-specific 3D spatial complementarity.

We further benchmarked MSIGN against traditional ML (RF and XGBoost), state-of-the-art DL (EHIGN and SS-GNN), and physics-based docking (AutoDock Vina) (Fig. 3E and Table S8). The results reveal a substantial accuracy gap. AutoDock Vina yielded the largest deviation (highest MAE), likely due to the challenges of standard scoring functions in modeling complex GPCR thermodynamics. General structure-based models like EHIGN and SS-GNN also exhibited large overestimation errors, confirming that models lacking domain-specific fine-tuning generalize poorly to novel SCs. While ligand-based ML models performed slightly better than general DL baselines, they still failed to achieve chemical accuracy.

(A) As illustrated by the MAE comparison (Fig. 3E, left), MSIGN stands out as the only methodology providing reliable, unbiased predictions. The sharp alignment between its predictions and experimental results (Fig. 3E, right) validates our “pre-training + full fine-tuning” paradigm. These findings underscore that the synergistic integration of multi-scale interaction modeling and domain-specific knowledge transfer is the key to bridging the gap between computational screening and experimental results in data-scarce scenarios.

3.8 Limitations of the study

Despite the robust performance of MSIGN, several limitations should be acknowledged. First, while our wet-lab validation on three novel synthetic cannabinoids yielded high consistency, the sample size remains limited for a comprehensive assessment of the model's performance in broader chemical spaces. Second, experimental binding assays (SPR and fluorescence) are subject to inherent variability and environmental factors, which may introduce minor measurement uncertainties. Third, although we benchmarked against AutoDock Vina, it represents a classical scoring function; more advanced but computationally expensive methods like FEP might provide different physical insights. Finally, this study focused specifically on the CB1 receptor. Whether the multi-scale priors and fine-tuning strategy generalize as effectively to the CB2 receptor or other GPCR families remains to be explored in future work.

4. Conclusion

In this study, we propose a binding affinity prediction model based on a multi-scale interaction graph neural network. Compared to other deep learning models, MSIGN achieves state-of-the-art performance across multiple evaluation metrics. This superior performance can be attributed to the feature extraction process of MSIGN, which not only incorporates physically meaningful covalent and non-covalent interactions but also integrates critical chemical prior knowledge, which is essential for accurate binding affinity prediction.

Furthermore, we demonstrate the effectiveness of the pre-training and fine-tuning paradigm in the context of binding affinity prediction using a SC dataset. Moreover, the choice of fine-tuning strategy—whether full fine-tuning or frozen fine-

tuning—has a substantial impact on model performance, depending on the characteristics of the downstream dataset. Specifically, on our SC dataset, full fine-tuning outperformed frozen fine-tuning, yielding more accurate predictions.

We believe that our MSIGN model provides a novel framework for researchers, offering a robust solution for achieving reliable binding affinity predictions even in scenarios where downstream task data are limited. This approach opens new avenues for advancing computational drug discovery and molecular design.

Author contributions

Jun Liao: conceptualization. Zhenyong Cheng: methodology. Dinghao Liu: software and writing – review & editing. Yuanpeng Fu: writing – original draft. Kewei Sheng: investigation. Yan Xing: formal analysis and data curation. Yanling Qiao: validation. Shangxuan Cai: validation. Jubo Wang: validation. Peng Xu: supervision and project administration.

Conflicts of interest

The authors declare no competing financial interest.

Data availability

The source code, trained models, and scripts used in this study are openly available on GitHub at <https://github.com/Dr-F-Arthur/MSIGN/tree/master>. An archived version of the repository is available on Zenodo under the identifier DOI: <https://zenodo.org/records/16018515>. The public datasets used for training and evaluation in this study are available from the following resources. PDBbind-v2020: <https://www.pdbbind-plus.org.cn/download>. CASF Benchmarks (2013/2016): <https://www.pdbbind-plus.org.cn/casf>. BindingDB: <https://www.bindingdb.org/rwd/bind/chemsearch/marvin/Download.jsp>.

Supplementary information is available (SI). See DOI: <https://doi.org/10.1039/d5dd00317b>.

Acknowledgements

This work was supported by Zhejiang Lab (Program: *Ab Initio* Design and Generation of AI Models for Small Molecule Ligands Based on Target Structures, Grant No. 2022PE0AC03), the National Key R&D Program of China (Program: A Study on the Diagnosis of Addiction to Synthetic Cannabinoids and Methods of Assessing the Risk of Abuse, Grant No. 2022YFC3300905), and the National Key R&D Program of China (Program: Research on Key Technologies for Monitoring and Identifying Drug Abuse of Anesthetic Drugs and Psychotropic Substances, and Intervention for Addiction, Grant No. 2023YFC3304200).

References

- 1 M. Ragoza, J. Hochuli, E. Idrobo, J. Sunseri and D. R. Koes, Protein–Ligand Scoring with Convolutional Neural



- Networks, *J. Chem. Inf. Model.*, 2017, 57(4), 942–957, DOI: [10.1021/acs.jcim.6b00740](https://doi.org/10.1021/acs.jcim.6b00740).
- 2 Z. Jin, T. Wu, T. Chen, D. Pan, X. Wang, J. Xie, L. Quan and Q. Lyu, CAPLA: Improved Prediction of Protein-Ligand Binding Affinity by a Deep Learning Approach Based on a Cross-Attention Mechanism, *Bioinformatics*, 2023, 39(2), btad049, DOI: [10.1093/bioinformatics/btad049](https://doi.org/10.1093/bioinformatics/btad049).
- 3 Z. Yang, W. Zhong, Q. Lv, T. Dong and C. Yu-Chian Chen, Geometric Interaction Graph Neural Network for Predicting Protein-Ligand Binding Affinities from 3D Structures (GIGN), *J. Phys. Chem. Lett.*, 2023, 14(8), 2020–2033, DOI: [10.1021/acs.jpcclett.2c03906](https://doi.org/10.1021/acs.jpcclett.2c03906).
- 4 X. Zhang, H. Gao, H. Wang, Z. Chen, Z. Zhang, X. Chen, Y. Li, Y. Qi and R. Wang, PLANET: A Multi-Objective Graph Neural Network Model for Protein-Ligand Binding Affinity Prediction, *J. Chem. Inf. Model.*, 2024, 64(7), 2205–2220, DOI: [10.1021/acs.jcim.3c00253](https://doi.org/10.1021/acs.jcim.3c00253).
- 5 Y. Zhang, S. Li, K. Meng and S. Sun, Machine Learning for Sequence and Structure-Based Protein-Ligand Interaction Prediction, *J. Chem. Inf. Model.*, 2024, 64(5), 1456–1472, DOI: [10.1021/acs.jcim.3c01841](https://doi.org/10.1021/acs.jcim.3c01841).
- 6 H. Öztürk, A. Özgür and E. OzKirimli, DeepDTA: Deep Drug-Target Binding Affinity Prediction, *Bioinformatics*, 2018, 34(17), i821–i829, DOI: [10.1093/bioinformatics/bty593](https://doi.org/10.1093/bioinformatics/bty593).
- 7 T. Nguyen; H. Le; T. P. Quinn; T. Nguyen; T. D. Le; S. Venkatesh GraphDTA: Predicting Drug-Target Binding Affinity with Graph Neural Networks.
- 8 M. Jiang, Z. Li, S. Zhang, S. Wang, X. Wang, Q. Yuan and Z. Wei, Drug-Target Affinity Prediction Using Graph Neural Network and Contact Maps, *RSC Adv.*, 2020, 10(35), 20701–20712, DOI: [10.1039/D0RA02297G](https://doi.org/10.1039/D0RA02297G).
- 9 T. M. Nguyen, T. Nguyen, T. M. Le and T. Tran, GEFA: Early Fusion Approach in Drug-Target Affinity Prediction, *IEEE Trans. Comput. Biol. Bioinform.*, 2022, 19(2), 718–728, DOI: [10.1109/TCBB.2021.3094217](https://doi.org/10.1109/TCBB.2021.3094217).
- 10 M. Jiang, S. Wang, S. Zhang, W. Zhou, Y. Zhang and Z. Li, Sequence-Based Drug-Target Affinity Prediction Using Weighted Graph Neural Networks, *BMC Genom.*, 2022, 23(1), 449, DOI: [10.1186/s12864-022-08648-9](https://doi.org/10.1186/s12864-022-08648-9).
- 11 H. Qi, T. Yu, W. Yu and C. Liu, Drug-Target Affinity Prediction with Extended Graph Learning-Convolutional Networks, *BMC Bioinf.*, 2024, 25(1), 75, DOI: [10.1186/s12859-024-05698-6](https://doi.org/10.1186/s12859-024-05698-6).
- 12 Y.-B. Wang, Z.-H. You, S. Yang, H.-C. Yi, Z.-H. Chen and K. Zheng, A Deep Learning-Based Method for Drug-Target Interaction Prediction Based on Long Short-Term Memory Neural Network, *BMC Med. Inform. Decis. Mak.*, 2020, 20(S2), 49, DOI: [10.1186/s12911-020-1052-0](https://doi.org/10.1186/s12911-020-1052-0).
- 13 S. Li, J. Zhou, T. Xu, L. Huang, F. Wang, H. Xiong, W. Huang, D. Dou and H. Xiong Structure-Aware Interactive Graph Neural Networks for the Prediction of Protein-Ligand Binding Affinity. *arXiv* 2021. preprint arXiv:10.48550/arXiv.2107.10670, DOI: [10.48550/arXiv.2107.10670](https://doi.org/10.48550/arXiv.2107.10670).
- 14 C. Xia, S.-H. Feng, Y. Xia, X. Pan and H.-B. Shen, Leveraging Scaffold Information to Predict Protein-Ligand Binding Affinity with an Empirical Graph Neural Network, *Briefings Bioinf.*, 2023, 24(1), bbac603, DOI: [10.1093/bib/bbac603](https://doi.org/10.1093/bib/bbac603).
- 15 R. Gorantla, A. Kubincová, A. Y. Weiße and A. S. J. S. Mey, From Proteins to Ligands: Decoding Deep Learning Methods for Binding Affinity Prediction, *J. Chem. Inf. Model.*, 2024, 64(7), 2496–2507, DOI: [10.1021/acs.jcim.3c01208](https://doi.org/10.1021/acs.jcim.3c01208).
- 16 J. Jiménez, M. Škalič, G. Martínez-Rosell and G. De Fabritiis, K_{DEEP} : Protein-Ligand Absolute Binding Affinity Prediction via 3D-Convolutional Neural Networks, *J. Chem. Inf. Model.*, 2018, 58(2), 287–296, DOI: [10.1021/acs.jcim.7b00650](https://doi.org/10.1021/acs.jcim.7b00650).
- 17 M. M. Stepniewska-Dziubinska, P. Zielenkiewicz and P. Siedlecki, Development and Evaluation of a Deep Learning Model for Protein-Ligand Binding Affinity Prediction, *Bioinformatics*, 2018, 34(21), 3666–3674, DOI: [10.1093/bioinformatics/bty374](https://doi.org/10.1093/bioinformatics/bty374).
- 18 F. Imrie, A. R. Bradley, M. Van Der Schaar and C. M. Deane, Protein Family-Specific Models Using Deep Neural Networks and Transfer Learning Improve Virtual Screening and Highlight the Need for More Data, *J. Chem. Inf. Model.*, 2018, 58(11), 2319–2330, DOI: [10.1021/acs.jcim.8b00350](https://doi.org/10.1021/acs.jcim.8b00350).
- 19 J. A. Morrone, J. K. Weber, T. Huynh, H. Luo and W. D. Cornell, Combining Docking Pose Rank and Structure with Deep Learning Improves Protein-Ligand Binding Mode Prediction over a Baseline Docking Approach, *J. Chem. Inf. Model.*, 2020, 60(9), 4170–4179, DOI: [10.1021/acs.jcim.9b00927](https://doi.org/10.1021/acs.jcim.9b00927).
- 20 H. Hassan-Harrirou, C. Zhang and T. Lemmin, RosENet: Improving Binding Affinity Prediction by Leveraging Molecular Mechanics Energies with an Ensemble of 3D Convolutional Neural Networks, *J. Chem. Inf. Model.*, 2020, 60(6), 2791–2802, DOI: [10.1021/acs.jcim.0c00075](https://doi.org/10.1021/acs.jcim.0c00075).
- 21 S. Moon, W. Zhung, S. Yang, J. Lim and W. Y. Kim, PIGNet: A Physics-Informed Deep Learning Model toward Generalized Drug-Target Interaction Predictions, *Chem. Sci.*, 2022, 13(13), 3661–3673, DOI: [10.1039/d1sc06946b](https://doi.org/10.1039/d1sc06946b).
- 22 Z. Yang, W. Zhong, Q. Lv, T. Dong, G. Chen and C. Y.-C. Chen, Interaction-Based Inductive Bias in Graph Neural Networks: Enhancing Protein-Ligand Binding Affinity Predictions From 3D Structures, *IEEE Trans. Pattern Anal. Mach. Intell.*, 2024, 46(12), 8191–8208, DOI: [10.1109/TPAMI.2024.3400515](https://doi.org/10.1109/TPAMI.2024.3400515).
- 23 W. Torng and R. B. Altman, Graph Convolutional Neural Networks for Predicting Drug-Target Interactions, *J. Chem. Inf. Model.*, 2019, 59(10), 4131–4149, DOI: [10.1021/acs.jcim.9b00628](https://doi.org/10.1021/acs.jcim.9b00628).
- 24 R. Milo; S. Shen-Orr; S. Itzkovitz; N. Kashtan; D. Chklovskii; U. Alon Network Motifs: Simple Building Blocks of Complex Networks.
- 25 S. Han, H. Fu, Y. Wu, G. Zhao, Z. Song, F. Huang, Z. Zhang, S. Liu and W. Zhang, HimGNN: A Novel Hierarchical Molecular Graph Representation Learning Framework for Property Prediction, *Briefings Bioinf.*, 2023, 24(5), bbad305, DOI: [10.1093/bib/bbad305](https://doi.org/10.1093/bib/bbad305).
- 26 H. Öztürk, E. OzKirimli and A. Özgür, WideDTA: Prediction of Drug-Target Binding Affinity, *arXiv*, 2019, preprint, DOI: [10.48550/arXiv.1902.04166](https://doi.org/10.48550/arXiv.1902.04166).
- 27 H. T. Rube, C. Rastogi, S. Feng, J. F. Kribelbauer, A. Li, B. Becerra, L. A. N. Melo, B. V. Do, X. Li, H. H. Adam,



- N. H. Shah, R. S. Mann and H. J. Bussemaker, Prediction of Protein–Ligand Binding Affinity from Sequencing Data with Interpretable Machine Learning, *Nat. Biotechnol.*, 2022, **40**(10), 1520–1527, DOI: [10.1038/s41587-022-01307-0](https://doi.org/10.1038/s41587-022-01307-0).
- 28 C. Cai, S. Wang, Y. Xu, W. Zhang, K. Tang, Q. Ouyang, L. Lai and J. Pei, Transfer Learning for Drug Discovery, *J. Med. Chem.*, 2020, **63**(16), 8683–8694, DOI: [10.1021/acs.jmedchem.9b02147](https://doi.org/10.1021/acs.jmedchem.9b02147).
- 29 R. Wang, X. Fang, Y. Lu, C.-Y. Yang and S. Wang, The PDBbind Database: Methodologies and Updates, *J. Med. Chem.*, 2005, **48**(12), 4111–4119, DOI: [10.1021/jm048957q](https://doi.org/10.1021/jm048957q).
- 30 T. Liu, L. Hwang, S. K. Burley, C. I. Nitsche, C. Southan, W. P. Walters and M. K. Gilson, BindingDB in 2024: A FAIR Knowledgebase of Protein–Small Molecule Binding Data, *Nucleic Acids Res.*, 2025, **53**(D1), D1633–D1644, DOI: [10.1093/nar/gkae1075](https://doi.org/10.1093/nar/gkae1075).
- 31 T. Hua, K. Vemuri, M. Pu, L. Qu, G. W. Han, Y. Wu, S. Zhao, W. Shui, S. Li, A. Korde, R. B. Laprairie, E. L. Stahl, J.-H. Ho, N. Zvonok, H. Zhou, I. Kufareva, B. Wu, Q. Zhao, M. A. Hanson, L. M. Bohn, A. Makriyannis, R. C. Stevens and Z.-J. Liu, Crystal Structure of the Human Cannabinoid Receptor CB1, *Cell*, 2016, **167**(3), 750–762.e14, DOI: [10.1016/j.cell.2016.10.004](https://doi.org/10.1016/j.cell.2016.10.004).
- 32 T. Hua, K. Vemuri, S. P. Nikas, Y. Wu, L. Qu, M. Pu, A. Korde, S. Jiang, J.-H. Ho, G. W. Han, K. Ding, X. Li, H. Liu, M. A. Hanson, S. Zhao, L. M. Bohn, A. Makriyannis, R. C. Stevens and Z.-J. Liu, Crystal Structures of Agonist-Bound Human Cannabinoid Receptor CB1, *Nature*, 2025, **646**(8085), 754–758, DOI: [10.1038/s41586-025-09454-5](https://doi.org/10.1038/s41586-025-09454-5).
- 33 X. Yang, X. Wang, Z. Xu, C. Wu, Y. Zhou, Y. Wang, G. Lin, K. Li, M. Wu, A. Xia, J. Liu, L. Cheng, J. Zou, W. Yan, Z. Shao and S. Yang, Molecular Mechanism of Allosteric Modulation for the Cannabinoid Receptor CB1, *Nat. Chem. Biol.*, 2022, **18**(8), 831–840, DOI: [10.1038/s41589-022-01038-y](https://doi.org/10.1038/s41589-022-01038-y).
- 34 J. Lim, S. Ryu, K. Park, Y. J. Choe, J. Ham and W. Y. Kim, Predicting Drug–Target Interaction Using a Novel Graph Neural Network with 3D Structure-Embedded Graph Representation, *J. Chem. Inf. Model.*, 2019, **59**(9), 3981–3988, DOI: [10.1021/acs.jcim.9b00387](https://doi.org/10.1021/acs.jcim.9b00387).
- 35 D. Jones, H. Kim, X. Zhang, A. Zemla, G. Stevenson, W. F. D. Bennett, D. Kirshner, S. E. Wong, F. C. Lightstone and J. E. Allen, Improved Protein–Ligand Binding Affinity Prediction with Structure-Based Deep Fusion Inference, *J. Chem. Inf. Model.*, 2021, **61**(4), 1583–1592, DOI: [10.1021/acs.jcim.0c01306](https://doi.org/10.1021/acs.jcim.0c01306).
- 36 J. Gilmer; S. S. Schoenholz; P. F. Riley; O. Vinyals; G. E. Dahl Neural Message Passing for Quantum Chemistry. *arXiv*, 2017, preprint arXiv:10.48550/arXiv.1704.01212 DOI: [10.48550/arXiv.1704.01212](https://doi.org/10.48550/arXiv.1704.01212).
- 37 H. Cai, H. Zhang, D. Zhao, J. Wu and L. Wang, FP-GNN: A Versatile Deep Learning Architecture for Enhanced Molecular Property Prediction, *Briefings Bioinf.*, 2022, **23**(6), bbac408, DOI: [10.1093/bib/bbac408](https://doi.org/10.1093/bib/bbac408).
- 38 Z. Zheng, Y. Tan, H. Wang, S. Yu, T. Liu and C. Liang, CasANGCL: Pre-Training and Fine-Tuning Model Based on Cascaded Attention Network and Graph Contrastive Learning for Molecular Property Prediction, *Briefings Bioinf.*, 2023, **24**(1), bbac566, DOI: [10.1093/bib/bbac566](https://doi.org/10.1093/bib/bbac566).
- 39 Z. Wang, M. Liu, Y. Luo, Z. Xu, Y. Xie, L. Wang, L. Cai, Q. Qi, Z. Yuan, T. Yang and S. Ji, Advanced Graph and Sequence Neural Networks for Molecular Property Prediction and Drug Discovery, *Bioinformatics*, 2022, **38**(9), 2579–2586, DOI: [10.1093/bioinformatics/btac112](https://doi.org/10.1093/bioinformatics/btac112).
- 40 L. Hirschfeld, K. Swanson, K. Yang, R. Barzilay and C. W. Coley, Uncertainty Quantification Using Neural Networks for Molecular Property Prediction, *J. Chem. Inf. Model.*, 2020, **60**(8), 3770–3780, DOI: [10.1021/acs.jcim.0c00502](https://doi.org/10.1021/acs.jcim.0c00502).
- 41 Z. Yang, W. Zhong, L. Zhao, Yu-C. Chen and C. MGraphDTA, Deep Multiscale Graph Neural Network for Explainable Drug–Target Binding Affinity Prediction, *Chem. Sci.*, 2022, **13**(3), 816–833, DOI: [10.1039/D1SC05180F](https://doi.org/10.1039/D1SC05180F).
- 42 S. Zhang, Y. Jin, T. Liu, Q. Wang, Z. Zhang, S. Zhao and B. Shan, SS-GNN: A Simple-Structured Graph Neural Network for Affinity Prediction, *ACS Omega*, 2023, **8**(25), 22496–22507, DOI: [10.1021/acsomega.3c00085](https://doi.org/10.1021/acsomega.3c00085).
- 43 Y. Li, Z. Liu, J. Li, L. Han, J. Liu, Z. Zhao and R. Wang, Comparative Assessment of Scoring Functions on an Updated Benchmark: 1. Compilation of the Test Set, *J. Chem. Inf. Model.*, 2014, **54**(6), 1700–1716, DOI: [10.1021/ci500080q](https://doi.org/10.1021/ci500080q).
- 44 M. Su, Q. Yang, Y. Du, G. Feng, Z. Liu, Y. Li and R. Wang, Comparative Assessment of Scoring Functions: The CASF-2016 Update, *J. Chem. Inf. Model.*, 2019, **59**(2), 895–913, DOI: [10.1021/acs.jcim.8b00545](https://doi.org/10.1021/acs.jcim.8b00545).
- 45 J. R. Ash, C. Wognum, R. Rodríguez-Pérez, M. Aldeghi, A. C. Cheng, D.-A. Clevert, O. Engkvist, C. Fang, D. J. Price, J. M. Hughes-Oliver and W. P. Walters, Practically Significant Method Comparison Protocols for Machine Learning in Small Molecule Drug Discovery, *J. Chem. Inf. Model.*, 2025, **65**(18), 9398–9411, DOI: [10.1021/acs.jcim.5c01609](https://doi.org/10.1021/acs.jcim.5c01609).
- 46 G. Durant, F. Boyles, K. Birchall, B. Marsden and C. M. Deane, Robustly Interrogating Machine Learning-Based Scoring Functions: What Are They Learning?, *Bioinformatics*, 2025, **41**(2), btaf040, DOI: [10.1093/bioinformatics/btaf040](https://doi.org/10.1093/bioinformatics/btaf040).
- 47 P. Avdiunina; S. Jamal; F. Gusev; O. Isayev All That Glitters Is Not Gold: Importance of Rigorous Evaluation of Proteochemometric Models. January 22, 2025. doi: DOI: [10.26434/chemrxiv-2025-vbmgc](https://doi.org/10.26434/chemrxiv-2025-vbmgc).
- 48 M. Blum, A. Andreeva, L. C. Florentino, S. R. Chuguransky, T. Grego, E. Hobbs, B. L. Pinto, A. Orr, T. Paysan-Lafosse, I. Ponamareva, G. A. Salazar, N. Bordin, P. Bork, A. Bridge, L. Colwell, J. Gough, D. H. Haft, I. Letunic, F. Llinares-López, A. Marchler-Bauer, L. Meng-Papaxanthos, H. Mi, D. A. Natale, C. A. Orengo, A. P. Pandurangan, D. Piovesan, C. Rivoire, C. J. A. Sigrist, N. ThanKi, F. Thibaud-Nissen, P. D. Thomas, S. C. E. Tosatto, C. H. Wu and A. Bateman, InterPro: The Protein Sequence Classification Resource in 2025, *Nucleic Acids Res.*, 2025, **53**(D1), D444–D456, DOI: [10.1093/nar/gkae1082](https://doi.org/10.1093/nar/gkae1082).



- 49 V. Isberg, S. Mordalski, C. Munk, K. Rataj, K. Harpsøe, A. S. Hauser, B. Vroiling, A. J. Bojarski, G. Vriend and D. E. Gloriam, GPCRdb: An Information System for G Protein-Coupled Receptors, *Nucleic Acids Res.*, 2016, **44**(D1), D356–D364, DOI: [10.1093/nar/gkv1178](https://doi.org/10.1093/nar/gkv1178).
- 50 D. G. Gibson, L. Young, R.-Y. Chuang, J. C. Venter, C. A. Hutchison and H. O. Smith, Enzymatic Assembly of DNA Molecules up to Several Hundred Kilobases, *Nat. Methods*, 2009, **6**(5), 343–345, DOI: [10.1038/nmeth.1318](https://doi.org/10.1038/nmeth.1318).
- 51 K. Yusa, L. Zhou, M. A. Li, A. Bradley and N. L. Craig, A Hyperactive *piggyBac* Transposase for Mammalian Applications, *Proc. Natl. Acad. Sci. U. S. A.*, 2011, **108**(4), 1531–1536, DOI: [10.1073/pnas.1008322108](https://doi.org/10.1073/pnas.1008322108).

